

Facilitating the propagation of spiking activity in feedforward networks by including feedback

Hedyeh Rezaei¹, Ad Aertsen², Arvind Kumar^{2,3}* Alireza Valizadeh^{1,4}*,

1 Department of Physics, Institute for Advanced Studies in Basic Sciences (IASBS), Zanjan, Iran

2 Faculty of Biology, and Bernstein Center Freiburg, University of Freiburg, Freiburg, Germany

3 Dept. of Computational Science and Technology, School of Computer Science and Communication, KTH Royal Institute of Technology, Stockholm, Sweden

4 School of Cognitive Sciences, Institute for Research in Fundamental Sciences (IPM), Niavaran, Tehran, Iran.

*These authors contributed equally to this work.

*Corresponding authors: arvkumar@kth.se, valizade@iasbs.ac.ir

Abstract

Transient oscillations in the network activity upon sensory stimulation have been reported in different sensory areas. These evoked oscillations are the generic response of networks of excitatory and inhibitory neurons (*EI*-networks) to a transient external input. Recently, it has been shown that this resonance property of *EI*-networks can be exploited for communication in modular neuronal networks by enabling the transmission of sequences of synchronous spike volleys ('pulse packets'), despite the sparse and weak connectivity between the modules. The condition for successful transmission is that the pulse packet (PP) intervals match the period of the modules' resonance frequency. Hence, the mechanism was termed *communication through resonance (CTR)*. This mechanism has three severe constraints, though. First, it needs periodic trains of PPs, whereas single PPs fail to propagate. Second, the inter-PP interval needs to match the network resonance. Third, transmission is very slow, because in each module, the network resonance needs to build-up over multiple oscillation cycles. Here, we show that, by adding appropriate feedback connections to the network, the CTR mechanism can be improved and the aforementioned constraints relaxed. Specifically, we show that adding feedback connections between two upstream modules, called the resonance pair, in an otherwise feedforward modular network can support successful propagation of a single PP throughout the entire network. The key condition for successful transmission is that the sum of the forward and backward delays in the resonance pair matches the resonance frequency of the network modules. The transmission is much faster, by more than a factor of two, than in the original CTR mechanism. Moreover, it distinctly lowers the threshold for successful communication by synchronous spiking in modular networks of weakly coupled networks. Thus, our results suggest a new functional role of bidirectional connectivity for the communication in cortical area networks.

Author summary

The cortex is organized as a modular system, with the modules (cortical areas) communicating via weak long-range connections. It has been suggested that the

intrinsic resonance properties of population activities in these areas might contribute to enabling successful communication. A module's intrinsic resonance appears in the damped oscillatory response to an incoming spike volley, enabling successful communication during the peaks of the oscillation. Such communication can be exploited in feedforward networks, provided the participating networks have similar resonance frequencies. This, however, is not necessarily true for cortical networks. Moreover, the communication is slow, as it takes several oscillation cycles to build up the response in the downstream network. Also, only periodic trains of spikes volleys (and not single volleys) with matching intervals can propagate. Here, we present a novel mechanism that alleviates these shortcomings and enables propagation of synchronous spiking across weakly connected networks with not necessarily identical resonance frequencies. In this framework, an individual spike volley can propagate by local amplification through reverberation in a loop between two successive networks, connected by feedforward and feedback connections: the resonance pair. This overcomes the need for activity build-up in downstream networks, causing the volley to propagate distinctly faster and more reliably.

Introduction

Anatomical differences and functional specialization of different brain regions suggest that the brain is organized as a highly modular system. This modularity can be observed in the neocortex at multiple spatial scales, ranging from inter-areal connectivity [1] to inter- and intra-layer connectivity within a single cortical column [2–5]. A modular design indeed provides numerous benefits, not only making the system scalable, but also rendering it with robustness to structural perturbations [6].

To exploit the modularity of the brain, it is however, necessary that neuronal spiking activity from one specialized network can be reliably transmitted to another network and that the downstream network is able to read the incoming activity [7, 8]. Therefore, understanding how spiking activity is reliably propagated from one brain region to another is crucial for understanding the functional organization and information processing in the brain.

Different brain modules, irrespective of their spatial scale (inter-areal or inter-layer), are interconnected by convergent-divergent connections. Typically, the connectivity between any two modular networks is sparse, and synapses are weak. Over the last decade, the problem of reliably transmitting spiking activity via weak and sparse connections has attracted much attention from experimentalists and theoreticians alike [7, 9–16]. If the inter-module networks under study exclusively include feedforward connections, the only way to overcome the problem of transmission with weak synapses is to provide more efficient signals by synchronizing the spike signals to be transmitted [17–19]. Neuronal signals in this case are considered as volleys of spikes (*pulse packets*) which can be quantified by the number of spikes in the volley ($\alpha = 50 - 100$ spikes) and their temporal dispersion ($\sigma \approx 1 - 10$ ms), measuring the degree of synchronization of the spiking activity in the volley [18, 20]. Several studies have demonstrated that the downstream effect of a pulse packet depends both on α and σ (see [7] for a review). Note that a pulse packet by itself does not carry any information; rather, the information resides in the combination of neurons participating in the spike volley, both in the sender and receiver networks [21].

Convergent-divergent connectivity is a very potent connectivity motif that can generate and amplify spiking synchrony by virtue of shared inputs [17–19, 21]. When inputs are sufficiently synchronous, the transmission speed is very high and governed only by synaptic delays. However, it has been shown that this mechanism requires relatively dense connectivity and/or highly synchronous inputs [7]. These two

requirements are inconsistent with available experimental data on both the neuronal
35
connectivity and activity across cortical areas.
36

But cortical networks are not strictly feedforward, and recurrent and feedback
37
connections are prevalent in the central nervous system [3,4]. Network activity dynamics
38
determined by recurrent connectivity have a strong effect on neuronal response
39
properties. For instance, network oscillations modulate the neurons' spiking threshold in
40
a periodic fashion. If two networks oscillate at the same frequency and phase (coherent
41
oscillations), the transient decrease in the effective spiking threshold of neurons in the
42
downstream network coincides with the transient increase of the spiking activity of the
43
sending network, facilitating the transmission of spiking activity [8–10, 12, 15, 16]. Thus,
44
communication through coherence (CTC) not only provides the means to communicate
45
from one network to another, but it also provides the means to control the
46
communication, because only networks with an appropriate phase synchrony with the
47
sender network can tune in to the spiking activity they receive. However, there are two
48
clear limitations to this mechanism: (1) Experimentally observed oscillations are not
49
stable over long enough times to support their role in communicating spiking
50
activity [22], and (2) The mechanisms by which two networks can generate coherent
51
oscillations have so far remained quite obscure (however, see [23, 24]).
52

Recently, Hahn and colleagues proposed another mechanism that does not require
53
coherent spontaneous oscillations in the sender and receiver networks [15]. For a wide
54
range of biologically plausible neuron and network parameters, excitatory-inhibitory
55
networks (*EI*-networks) show features of network resonance. In this regime, the baseline
56
activity of the network itself is not oscillatory, but when perturbed with a transient
57
input, the network responds with a damped oscillation. When stimulated with a
58
periodic external input with the appropriate frequency, within a few oscillation cycles
59
the network starts to oscillate at its intrinsic oscillation frequency.
60

Thus, even a weak periodic input, provided it has the right frequency, exposes the
61
network resonance and creates oscillations in the receiver network which would not
62
exhibit oscillations otherwise. Network oscillations created through this resonance
63
phenomenon periodically lower the spike threshold of neurons in the receiver network,
64
allowing for a gradual build-up, over several oscillation cycles, for enabling the
65
transmission of the incoming activity. Therefore, this mechanism was termed
66
communication through resonance (CTR) [15]. Because oscillations only arise upon
67
appropriate stimulation of the downstream network, the oscillations in the sender and
68
receiver networks are automatically phase synchronized and, hence, facilitate the
69
transmission of the spiking activity involved in the stimulation. Thus, the *CTR*
70
mechanism resolves a fundamental problem of the *CTC* hypothesis: how to obtain and,
71
even more so, maintain phase synchrony between the network oscillations. Yet, at the
72
same time it creates new problems: First, it precludes the transmission of individual
73
pulse packets and, second, because the periodic stimulation activity needs to be
74
amplified by build-up over multiple oscillation cycles, communication through resonance
75
is prohibitively slow. Finally, it is not known how the inter-pulse interval of the external
76
signal can be matched the period of the evoked oscillations of the modules.
77

Here, we report the results of an investigation how the transmission of spiking
78
activity in a feedforward network (FFN), based on the CTR mechanism, can be
79
improved by adding appropriate feedback connections. To this end, we studied the
80
possibility of transmitting a single pulse packet in an FFN of *EI*-networks in which the
81
first two layers of *EI*-networks were bidirectionally connected via weak and sparse
82
excitatory synapses. We refer to these two bidirectionally coupled *EI*-networks as the
83
resonance pair. We found that adding such a resonance pair to an otherwise feedforward
84
modular network enabled fast transmission (in only two oscillation cycles) of a single
85
pulse packet through a built-in CTR mechanism, provided the sum of the feedforward
86

and feedback delays between the resonance pair matches the period of the resonance of the *EI*-networks. In the FFN with a resonance pair, the incoming single pulse packet initiated a periodic pulse packet train with appropriate timing (determined by the resonance frequency of the *EI*-networks), which was reliably transmitted through the remainder of the layered network of *EI*-networks. We found that the build-up of the network resonance was much faster in networks with a resonance pair: embedding a single resonance pair in a feedforward network increased the speed of CTR-based transmission by a factor of 2. Using numerical simulations, we identified conditions (strength, number and delay of the bidirectional connections) that ensured a stable transmission of the activity, without destabilizing the activity dynamics within the individual *EI*-networks in the layered network. We hypothesize that, since bidirectional connections between cortical areas are quite ubiquitous (e.g. [25–30]), such bidirectionally connected areas may provide good broadcasters of information in the brain at intermediate and large scales.

Methods

Neuron and synapse model

Neurons were modeled as leaky integrate-and-fire (LIF) neurons. The sub-threshold dynamics of the neuron's membrane potential were described by:

$$C_m \dot{V}_m = -G_{leak}[V_m(t) - V_{reset}] + I_{syn}(t) \quad (1)$$

where V_m denotes the membrane potential, C_m the membrane capacitance, G_{leak} the membrane leak conductance, and I_{syn} the total synaptic input current. When the membrane voltage reached the threshold of $V_{th} = -54$ ms, a spike was emitted and the potential was reset and clamped to $V_{reset} = -70$ mV for a refractory period ($t_{ref} = 2$ ms). To avoid a transient network synchrony at the beginning of the simulation, the initial membrane voltage of neurons was drawn from a normal distribution (mean: -70 ; standard deviation: 3 mV). The neuron model parameters are listed in Table 1.

Synaptic inputs were introduced by a transient change in the synaptic conductance G_{syn} :

$$I_{syn}(t) = G_{syn}(t)[V_m(t) - E_{syn}] \quad (2)$$

in which E_{syn} denotes the synaptic reversal potential. Conductance changes were modeled as alpha functions:

$$G_{syn}(t) = \frac{t}{\tau_{syn}} \exp\left(-\frac{t}{\tau_{syn}}\right) \quad (3)$$

where τ_{syn} is the synaptic time constant. The synapse model parameters are listed in Table 2. Synaptic transmission delays were set to 1.5 ms for within-layer connections; whereas inter-layer transmission delays were systematically varied as one of the key parameters in our study (as mentioned in the corresponding Figure captions).

Network connectivity

The network consisted of 10 layers, each one comprising 200 excitatory and 50 inhibitory neurons in the form of an *EI*-network (**Figure 1**). The connectivity within the layers (*EI*-networks) was chosen to be random with a fixed connection probability of 0.2 for all types of connections. For the inter-layer connectivity, we assumed that only the excitatory neurons from one layer *EI*-network projected to the excitatory neurons in

the following layer *EI*-network. From each layer, 70 randomly selected neurons projected to the next layer with connection probability of = 0.2. Thus, each neuron in a layer received on average 40 excitatory inputs from neurons within the layer network and 14 excitatory inputs from neurons in the preceding layer network. Synapses from a neuron onto itself were excluded, but multiple synapses between neurons were allowed. Inter-layer excitatory connections were set to be as strong as within-layer excitatory to excitatory connections. Further details of the model network parameters are listed in Table 3.

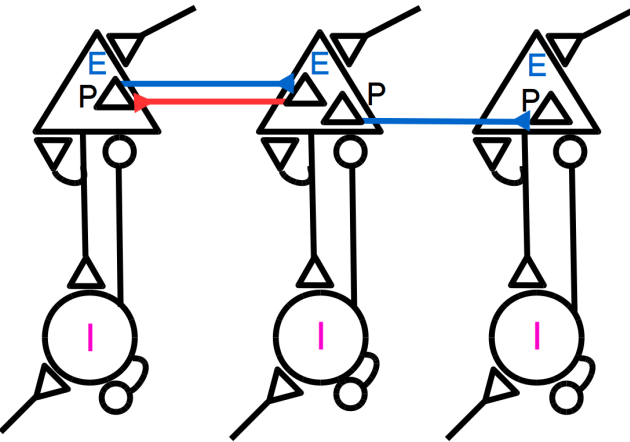


Fig 1. Schematic representation of a feedforward network with a resonance pair. 200 excitatory neurons in each layer (E), including 70 projecting neurons (P), and 50 inhibitory neurons (I) have random homogeneous sparse recurrent connections. Ten layers are connected sparsely through *EE* connections, indicated by blue arrows, in a feedforward manner. The red arrow from layer 2 to 1 indicates sparse random feedback connections from the second to the first layer *EI*-network, for which we used the term **resonance pair**.

External input

Each excitatory neuron in each layer *EI*-network was driven by 8,000 independent Poisson excitatory spike trains, each with a mean rate of 1 spike/s. Each inhibitory neuron in each layer *EI*-network was driven by 6,300 independent Poisson excitatory spike trains, at the same mean rate. In **Figures 7a,b**, the rate of the Poisson input to the *E*-neuron population was systematically varied, and for the *I*-neuron population the rate was adjusted accordingly, to keep the difference between the mean input rates to *E*- and *I*-neurons, 1,700 spikes/s, constant.

The synchronous input stimulus was a single pulse packet, injected into the projecting neurons in the first layer network. It consisted of a fixed number of spikes (α), distributed randomly around the packet's arrival time (t_n). The time of individual spikes were drawn independently from a Gaussian distribution centered around t_n , with a standard deviation of $\sigma = 2$ ms. In **Figure 6**, the external input for the FFN was a periodic train of pulse packets with inter-packet intervals of 25 ms. In **Figure 6c**, α was a control parameter and was varied systematically. In all remaining cases we used $\alpha = 20$.

Data analysis

Pairwise correlations

To estimate pairwise correlations, we divided the time into bins of size $\Delta t = 5$ ms, and transformed population spike trains to spike count vectors $y_i(t)$, using a rectangular kernel. The pairwise Pearson correlation coefficients were calculated as:

$$r_{ij} = \frac{\mathbb{E}[(y_i(t) - \bar{y}_i(t))(y_j(t) - \bar{y}_j(t))]}{\sigma_i \sigma_j} \quad (4)$$

where \mathbb{E} denotes the expectation value, σ the standard deviation, and barred values denote the means of variables. We averaged the r_{ij} over all pairs within a layer network to obtain the average synchrony within the layer. Correlation coefficients were computed from simulations with a duration of 20 sec and were averaged over 20 trials.

Population Fano Factor

To classify the population activity based on synchrony in the background activity, we measured the population Fano factor (pFF). To this end, we used spike count vectors ($y(t)$) of all excitatory neurons in a layer network and defined the pFF as:

$$pFF = \frac{VAR[y(t)]}{MEAN[y(t)]} \quad (5)$$

Network Frequency and Spectral Entropy

The network frequency is defined as the peak frequency of the Fourier transform of the spike count vectors $Y(f)$. To differentiate between asynchronous, aperiodic and oscillatory states of the two resonance pair networks, we measured the spectral entropy of one of the two EI -networks involved. We first calculated the power spectrum $S(f) = |Y(f)|^2$ and defined:

$$P(f) = \frac{S(f)}{\sum_m S(m)}, \quad (6)$$

Because $P(f)$ has unit area, we treated it as if it were a probability density and estimated its entropy. Our reasoning was that if a signal is periodic, all its power will be concentrated in a single frequency, resulting in a zero entropy. By contrast, when the signal power is uniformly distributed over all frequencies, the entropy will assume a maximal value. Given that we estimated the spectrum for a fixed number of frequency data points, we needed to normalize the entropy according to the number of frequency bins. Because here we took the normalized power spectrum as a proxy for the probability density, we refer to this measure as spectral entropy. The normalized spectral entropy is then defined as:

$$H = -\frac{\sum_{f=1}^N P(f) \log_2 P(f)}{\log_2 N}, \quad (7)$$

where N is the number of frequency data points. The denominator, $\log_2 N$ is the maximal spectral entropy, that is, the spectral entropy of white noise. Low entropy indicates temporal order of the population activity, i.e., an oscillatory state, whereas large values of H indicate an asynchronous state.

Signal-to-Noise Ratio

To distinguish successful propagations of single pulse packets from failed propagations, we estimated the *Signal-to-Noise Ratio (SNR)*, measuring the ratio of the variance of the averaged membrane potential of neurons in the tenth (final) layer network upon pulse packet injection into the first layer network, normalized by its variance during ongoing network activity:

$$SNR = \frac{VAR[y^{stim}(t)]}{VAR[y^{ongoing}(t)]} \quad (8)$$

Simulation tools

Network simulations were performed using the simulation tool NEST (<http://www.nest-initiative.org>) [31,32], interfaced with PyNest. The differential equations were integrated using fourth-order Runge-Kutta with a time step of 0.1 ms.

Results

We studied the effect of adding feedback connections between the first two layers in an otherwise feedforward modular network of *EI*-networks on the propagation of synchronous spiking activity along the network. Specifically, we compared the response of a purely feedforward network (FFN) with the response of a resonance pair network (RPN) to a variety of input stimulus conditions. To construct the RPN, we added feedback connections between the first two layers of the original FFN. The FFN consisted of 10 layers, each one consisting of a recurrent *EI*-network comprising 200 excitatory and 50 inhibitory neurons (**Figure 1**, see **Methods**). The external input and the excitation-inhibition ratio in the *EI*-networks were adjusted to set the baseline activity of the networks in an asynchronous-irregular state [33,34], characterized by highly irregular inter-spike intervals, low pairwise correlations, and weak network synchrony (as depicted in **Supplementary Figure S1**, see also **Methods**).

Pulse packet propagation

We first tested the propagation of synchronous spiking activity by stimulating the FFN with a single pulse packet ($\alpha = 20$ spikes, $\sigma = 2$ ms). This mimicked earlier simulation experiments [15,18,35], but with different FFN parameters. Given the weak projecting synapses and sparse inter-layer connectivity, this weak pulse packet failed to propagate along the feedforward network (**Figure 2a-c**). The injection of a pulse packet into the first layer network resulted in a clear but weak spike response in that layer, a much weaker response in the second layer (**Figure 2b**), and no tangible response in any of the subsequent layer networks. This failure to propagate was confirmed by the low signal-to-noise ratio in the 10th layer network ($SNR < 4$). Consistent with the weak spiking responses, there was no visible trace of the pulse packet in the subthreshold membrane potentials beyond the second layer (**Figure 2c**).

Next, we tested the propagation of a periodic train of pulse packets, each with the same characteristics as the single pulse packet described above. Consistent with previous results [15], such a periodic input successfully propagated along the feedforward network using the network resonance mechanism (**Figure 2e,f**, 10th layer $SNR = 4.5$). However, while the periodic pulse packet train did indeed successfully propagate to the last layer, this propagation was very slow. Thus, a distinct pulse packet response was observed there only after some 15 input cycles (**Figure 2f**), highlighting once more the

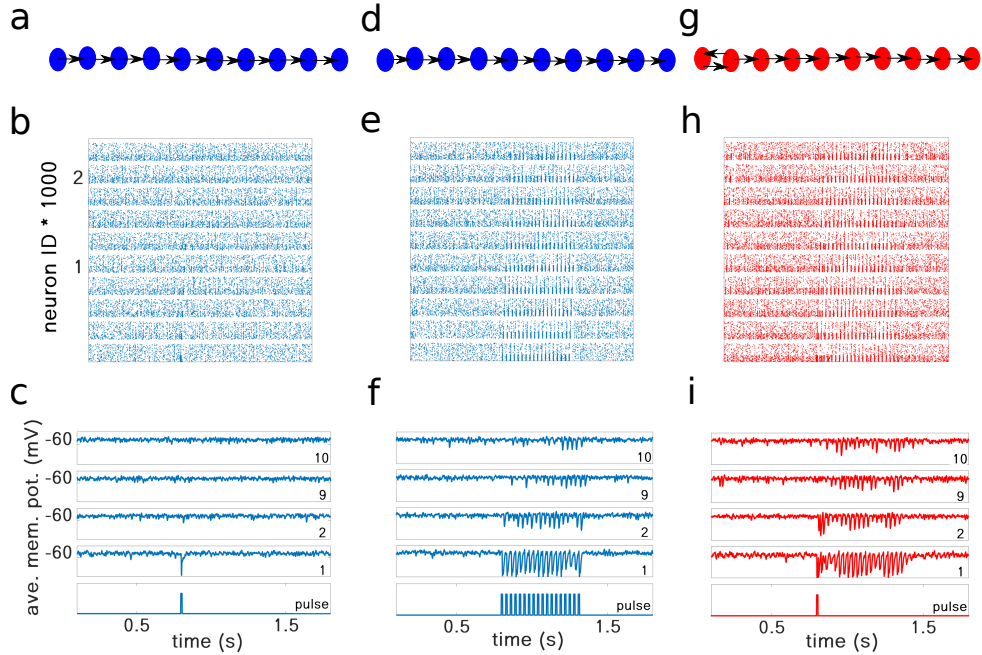


Fig 2. Comparison of the propagation of synchronous spiking in a feedforward network (FFN) and in a resonance pair network (RPN). The FFN failed to propagate a single pulse packet (a-c), whereas it did propagate a periodic train of pulse packets with the appropriate time interval between successive pulse packets (d-f). By contrast, the RPN, when stimulated with a single pulse packet, was able to propagate it successfully, provided that the inter-layer delay of the resonance pair matched the resonance period of the *EI*-networks involved (g-i). In the simulation experiment shown in panels (h) and (i), the loop transmission delay, defined as the sum of the forward and feedback transmission delays, was equal to the period of the pulse packet train in (e) and (f). The network structure for each column is plotted schematically in panels (a, d, g), the corresponding raster plots are shown in panels (b, e, h) for each stimulus condition. The average membrane potentials of the first two and last two layers in each of three simulation experiments are shown in panels (c, f, i), marked with layer numbers in each window, with the injected pulse packet shown in the bottom trace. Red color is used for the RPN, and blue for the FFN. Inter-pulse interval in panels (d-f) was 25 ms and the forward and backward delays in panels (g-i) were equal to 12.5 ms

key problem associated with the CTR mechanism. The reason for this is that each layer takes 2 – 3 cycles to build up strong enough oscillations of the membrane potentials in the next layer neurons to generate a reliable spike response.

To facilitate the propagation of a single pulse packet and to increase the speed of the resonance build-up in a layer of the FFN, we tested the idea of connecting the first and second layers in a bidirectional manner. To implement such a connectivity, we randomly selected 70 excitatory neurons from the second layer and projected them back to 70 randomly selected excitatory neurons in the first layer (**Figure 2g**). We made sure that the 70 neurons that projected back to the first layer were different from those that projected forward to the third layer. The synaptic strength, transmission delay, and connection probability of the feedback projections were all identical to those of the forward projections unless otherwise is mentioned in each Figure caption. We refer to

the two bidirectionally connected layer networks as the *resonance pair*. Interestingly,
236
the injection of a single pulse packet into the resonance pair network (RPN) was
237
sufficient to initiate transient oscillations in the first and second layer networks. The
238
bidirectional excitatory connectivity between the two layers rapidly amplified these
239
oscillations which, once sufficiently amplified, successfully propagated to all subsequent
240
layer networks (**Figure 2h,i**, 10th layer $SNR = 6.5$).
241

The *EI* balance in each layer of the network prevented it from developing sustained
242
oscillations. The oscillation duration across trials followed a gamma distribution,
243
showing that most of the oscillations survived for only some 8 – 10 cycles (**Figure 3**).
244
These results show that only a small change in the overall network architecture can
245
enable propagation of a single pulse packet using CTR, without driving the system into
246
sustained oscillations.
247

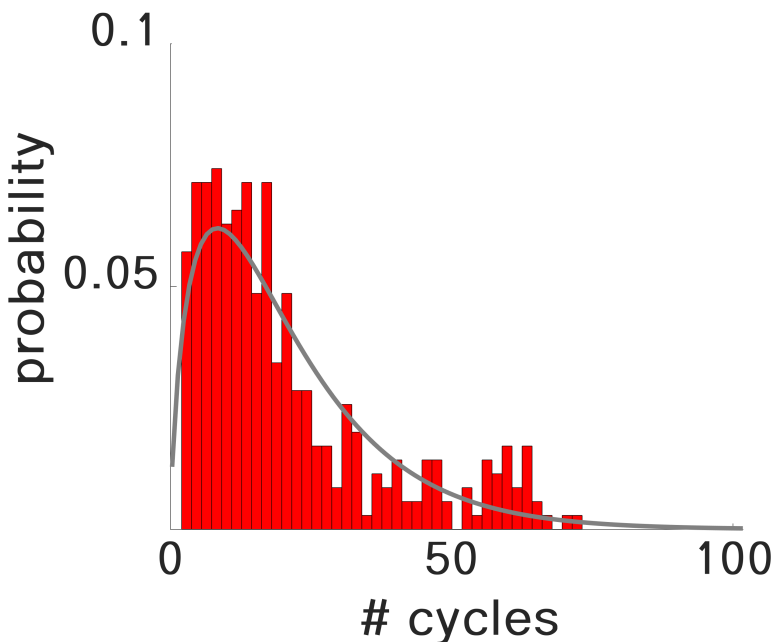


Fig 3. Distribution of the durations of oscillatory activity in the RPN upon injection of a single pulse packet. The RPN, when operating in a successful propagation mode, was able to quench the stimulus-induced oscillations after several oscillation cycles. The distribution of oscillation durations (shown in units of oscillation cycle) followed a Gamma distribution (fitted curve in gray). These data were collected from 350 trials with $SNR \geq 4.0$, i.e., for successful pulse packet propagations.

Inter-layer delays and connection strengths

The loop transmission delay and the inter-layer connection strength are two important structural parameters of the resonance pair. Together, they determine whether a single pulse packet can create transient oscillations and propagate the activity along the RPN. To characterize the effect of these two parameters, we systematically varied each of them and measured the resulting SNR in the tenth layer of the RPN (**Figure 4**). First, we varied both the delay and the synaptic strength of the connections between the layers (**Figure 4a**). Here, we set both the delay and strength of the feedback projections to be identical to those of the feedforward projections. We found that the input pulse packets propagated most successfully when the inter-layer delay was about
248
249
250
251
252
253
254
255
256
257

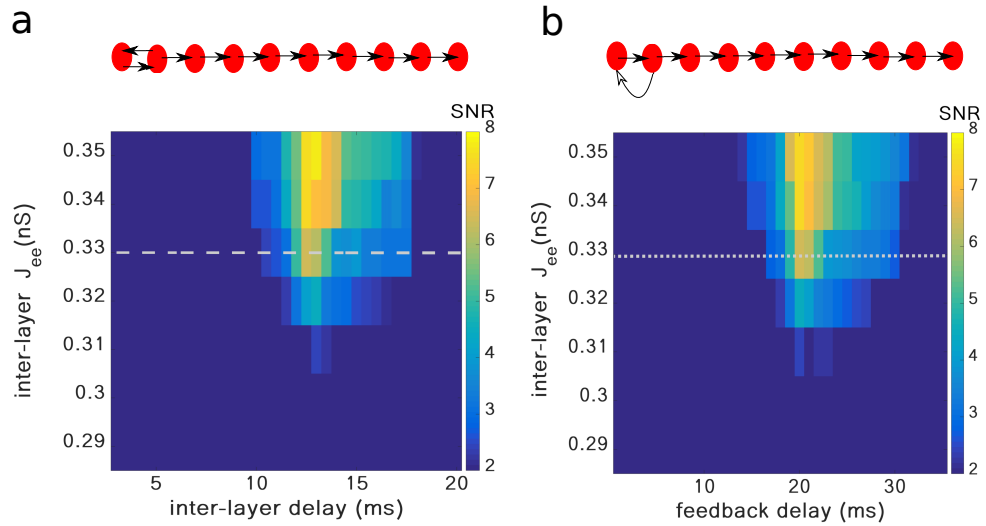


Fig 4. Signal-to-noise ratio (SNR) for 10th layer in the RPN depends on inter-layer delays and connection strengths of the resonance pair. (a) Delays for feedforward and feedback connections were set equal to each other and were systematically varied along the X-axis. Note that the most successful propagation was observed for a total loop delay (forward plus feedback delay) of 25 ms, matching the period of the intrinsic resonance oscillation of each individual layer *EI*-network (resonance frequency of 40 Hz). The range of inter-layer delays for which propagation was successful expanded as the inter-layer connections were strengthened. However, the *SNR* was still considerable for weaker ones. (b) Delays for feedforward connections were fixed to 5 ms, and for feedback connections were systematically varied along the X-axis. Again, the most successful propagation was observed for a total loop delay of 25 ms, matching each individual layer *EI*-network's resonance frequency of 40 Hz. In the schematic representations of the network structure (top panels), the length of the arrows indicate the duration of inter-layer delays. The dashed and dotted horizontal lines in (a) and (b) indicate the value of J_{ee} used to represent successful propagations in other figures.

12.5 ms. As the inter-layer connection strength was increased, the range of inter-layer delays for which the input pulse could propagate also increased (**Figure 4a**). With 12.5 ms inter-layer delay, the total loop delay for the resonance pair was 25 ms. Not surprisingly, this loop delay matched the period of the intrinsic network oscillations (corresponding to the resonance frequency of 40 Hz) of each individual layer *EI*-network.

Next, we fixed the feedforward delays at 5 ms and varied the delays of the feedback projections from layer 2 to layer 1. We found that in this case the feedback delay should be ≈ 20 ms to enable most successful propagation (**Figure 4b**). That is, most successful propagation again occurred when the loop delay (forward plus feedback delay) was 25 ms, again matching the resonance frequency (40 Hz) of the individual layer *EI*-networks.

To find the range of feedback and feedforward delays for which inputs could propagate, we varied each of these two delays independently, while keeping the inter-layer connection strength as ($J_{ee} = 0.33$ nS, **Figure 5**). We found that propagation was successful for a wide range of individual feedforward and feedback delays. Once again, it was most successful if the sum of the two delays (the loop delay) matched the period of the intrinsic network oscillations (here: 25 ms) of the individual layer *EI*-networks. These results confirm that successful signal propagation primarily

276
277

depends on the resonance pair's loop delay, i.e., the sum of the forward and feedback transmission delays.

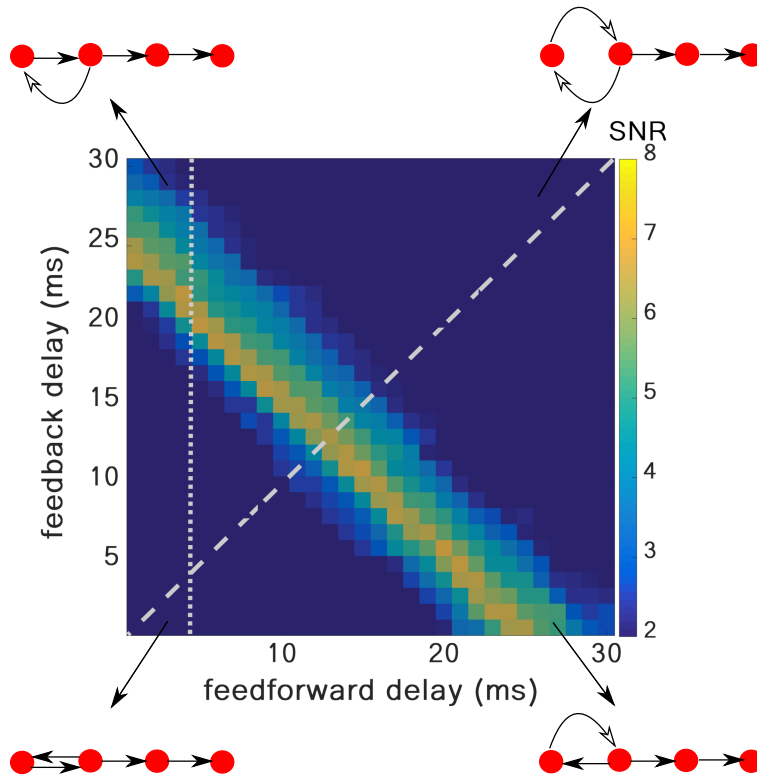


Fig 5. Signal-to-noise ratio (SNR) for 10th layer in the RPN for independently varied feedforward and feedback delays. The sum of the feedforward and feedback delays is the key parameter to enable signal propagation. When the inter-layer connection strength, J_{ee} , was fixed at 0.33 nS, most successful propagation was obtained for the condition that the sum of forward and feedback delays, rather than any of their individual values, matched the resonance period of the individual layer *EI*-network's resonance frequency of 40 Hz. In the schematic representations of the networks, only the first four layers are depicted, with the length of the arrows representing the delays between the resonance pair layer networks.

278
279
280
281
282
283
284
285
286
287
288
289

Resonance pair improves both the threshold and speed of propagation of synchronous spiking activity

Next, we addressed the question to what extent the inclusion of feedback *EE* connections between the first two layer networks of the FFN affects the threshold and speed of propagation of pulse packets in the network. To this end, we compared both the speed and *SNR* of the pulse packet response in the FFN and the RPN. For this comparison, we stimulated the RPN with a single pulse packet, whereas the FFN was stimulated with a periodic train of pulse packets (**Figures 6a,b**). The loop delay of the resonance pair in the RPN and the inter-pulse intervals in the periodic stimulation of the FFN were matched the resonance period of the *EI*-networks in the resonance pair, layers 1 and 2. We found that introducing feedback projections substantially increased the *SNR* of the pulse packet response in the RPN as compared to that in the FFN

290
291
292
293

(Figure 6c). This meant that much weaker pulse packets could propagate in the RPN than in the FFN. Thus, adding sparse *EE* feedback connections between only the first two layers of the FFN significantly reduced the threshold (minimum value of pulse packet strength α) for successful propagation throughout the entire FFN.

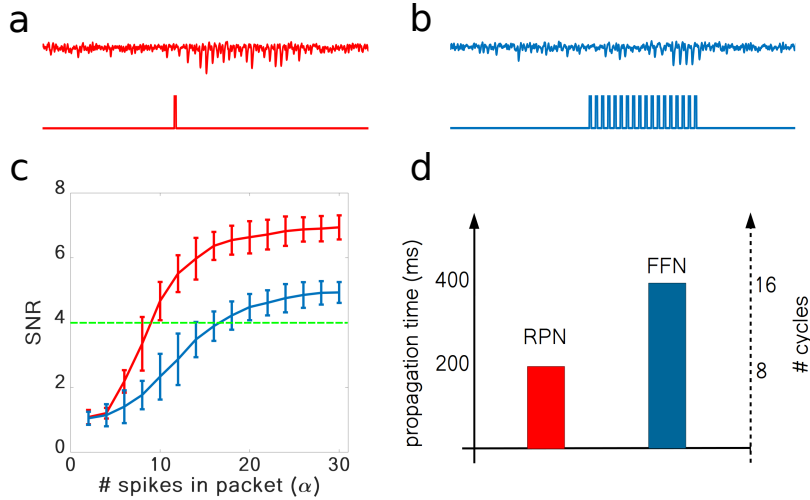


Fig 6. Introducing a resonance pair improves both the threshold and speed of propagation of synchronous spiking. (a) Averaged membrane potential of *E* neurons in the 10th layer in response to a single pulse packet (depicted in bottom trace) in the RPN, in the presence of feedback projections from layer 2 to layer 1. (b) Averaged membrane potential of *E* neurons in the 10th layer in response to a periodic pulse packet (depicted in bottom trace) in the FFN, in the absence of feedback projections. (c) *SNR* in the 10th layer of the RPN (red curve) and FFN (blue curve) as a function of strength, α , of the input pulse packet. Increasing α increased the *SNR* for both RPN and FFN. However, the red curve crosses the green dashed line (as an arbitrary threshold for successful propagation) at a clearly smaller value of α than the blue curve, implying clearly lower threshold of synchrony propagation in the RPN. (d) On average, synchronous activity propagates much faster in the RPN, by at least a factor of two, than in the FFN.

Next, we compared the propagation velocities in the RPN and the FFN. For a fair comparison of propagation speed in these two networks, we set the forward transmission delays to 5 ms in both networks. Therefore, to meet the condition that the loop delay in the resonance pair should match the intrinsic resonance in the participating *EI*-networks, the feedback delay was set to 20 ms in the RPN. In the FFN, as noted before, the pulse packet needed to be recreated by gradual build-up in each layer successively. Hence, it took on average between 2 – 4 oscillation cycles in each layer, before the pulse packet successfully reached the next layer. As shown in **Figure 6d**, the bidirectional projections between the first two layers in the RPN sufficed to rapidly amplify the network response, and, hence, there was no need to gradually build-up and recreate the pulse packet in each individual layer. As a result, the transmission in the RPN was much faster, by at least a factor of two, than in the FFN. These results demonstrate that introducing sparse feedback projections from layer 2 to layer 1 in an FFN with weak and sparse connections substantially accelerates the propagation of synchronous spiking in such network, thereby alleviating a significant problem associated with the mechanism of *communication through resonance*.

294
295
296
297
298
299
300
301
302
303
304
305
306
307
308
309

Network background activity

For stable propagation of synchronous spiking activity, it is important that the ongoing activity of the network remains stable and exhibits an asynchronous-irregular state without population activity oscillations [35]. In principle, the feedback projections in the resonance pair could destabilize the asynchronous-irregular activity state, induce spontaneous oscillations, and lead to the propagation of random fluctuations in the network activity. Therefore, we measured the effect of the feedback and feedforward projections on the network background activity. The strengths of feedforward and feedback connections in the RPN were set to be identical. First, we systematically varied the inter-layer connection strength and the rate of external (excitatory) input, and measured the population activity synchrony (population Fano factor, pFF) for the 10th layer of both the RPN and the FFN (**Figure 7a,b**). We also compared the firing rates, the irregularity of spike timing (CV) and the pairwise correlations for three different choices of these two parameters (**Supplementary Figure S1**).

We found that for weak external inputs, the background network activity remained in an asynchronous-irregular regime in both the RPN and FFN for a wide range of inter-layer connection strengths (**Figures 7a,b**). Likewise, for weaker inter-layer connections, the background network activity of both the RPN and FFN remained in an asynchronous-irregular regime. However, when both external input and inter-layer connections were strong, large fluctuations induced by the external input could propagate to downstream layers. Propagation of such spurious fluctuations resulted in synchronous-irregular activity in the downstream networks (**Figures 7a,b**, and **Supplementary Figure S1**; raster plots are also depicted in **Supplementary Figure S2**). Such undesirable emergence of synchrony in the background network activity because of stronger inter-layer connections and stronger external input was observed in both the RPN and FFN. However, in the RPN this transition to synchronous-irregular background activity occurred at clearly lower values of external inputs and inter-layer connection strengths than in the FFN (compare **Figures 7a,b**). That is, while the resonance pair reduced the threshold for propagation and accelerated the pulse packet propagation, it also constrained the range of network and input parameters for which stable propagation could be observed.

To determine the degree of synchrony in the background network activity for different inter-layer connection strengths and delays, we measured the population Fano factor (cf. Methods) for both the RPN and FFN networks, with the input rate set to 8 kHz (**Figures 7c,d**). These results demonstrate that the inter-layer delay plays no role in inducing synchrony in the FFN background network activity (**Figure 7d**). However, it does render a regime for eliciting synchronous background activity in an RPN (**Figure 7c**). This regime existed for the range of delays that matched the resonance period of the *EI*-networks involved, and for stronger inter-layer connections it increased significantly. Therefore, the parameter values causing this synchronous regime in the RPN background activity should be carefully avoided, because this regime prohibits reliable signal propagation.

Conditions for resonance in the resonance pair

The connectivity between the layers of the resonance pair could affect the propagation of synchronous spiking in the RPN in different ways. It could prohibit the propagation of pulse packets by enabling spurious network fluctuations to propagate, or by altering the resonance properties of the two layer networks involved. Whereas weak connectivity may not allow the resonance to occur, strong connectivity could induce spontaneous network oscillations, precluding the resonance-based mechanism from supporting the propagation of pulse packets. Therefore, we systematically varied both the forward and

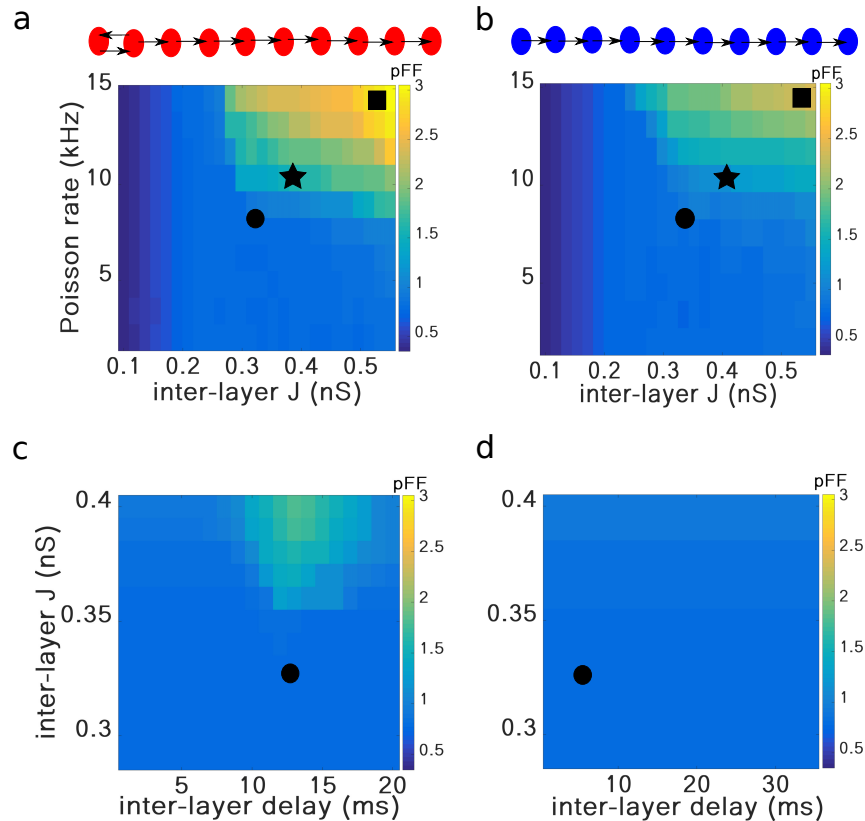


Fig 7. Different background activity regimes in the RPN (a, c) and FFN (b, d) networks. The population Fano factor in the 10th layer of the RPN (a) and FFN (b), is shown as a measure of synchrony in the background network activity for different strengths of inter-layer connections (X-axis) and input rate (Y-axis). The cyan area, indicated by an asterisk, denotes a synchronous irregular regime, whereas the vast, blue area denotes the asynchronous irregular regime, with a long-tailed distribution of CV_{ISI} and low average correlation coefficients (Supplementary Figure S1). Both network types transit to the synchronous irregular regime, indicated by a black square, with increasing input rate and inter-layer connection strength. However, the RPN reaches the synchronous irregular state much earlier than the FFN. The population Fano factor in the 10th layer of the RPN (c) and FFN (d), is shown for different inter-layer connection delay (X-axis) and strength (Y-axis). The input rate was set to 8 kHz for both network types. For strong enough inter-layer connections, provided their loop delay matched the resonance period of the network, sustained background activity oscillations might develop in the network and propagate to the downstream layers. Black circles in all four panels indicate the parameter settings used to investigate the pulse packet propagation in Figures 2, 3 and 6. In panels (a) and (b), the feedforward and feedback delays were set to 5 ms, respectively.

feedback connectivity between the two layers and determined the regime most suitable for communication through resonance (Figure 8). We found that an increase in either the connection probabilities (Figure 8a,b) or connection strengths (Figure 8c,d) increased the network's propensity to oscillate. Strong feedback connections and high connection probabilities induced spontaneous oscillations in both layer networks. The diagonal symmetry of Figure 8a,b (and to a lesser extent in Figure 8c,d) shows that the feedback connections can compensate for a lack of feedforward connections (as in

360
361
362
363
364
365
366

367
368
369
370
371
372
373

Figure 8a,b, or their weakness (as in **Figure 8c,d**). For moderate values of the feedback connection probability and connection strength, there is a region in the parameter space for which single pulse packets can be propagated by exploiting the network resonance property, without destabilizing the network activity dynamics into sustained network oscillations. This region is distinguished by a *pFF* of about 1, the blue area in **Figure 8a,b**, and an example of it is marked with a black circle in all four panels of **Figure 8**.

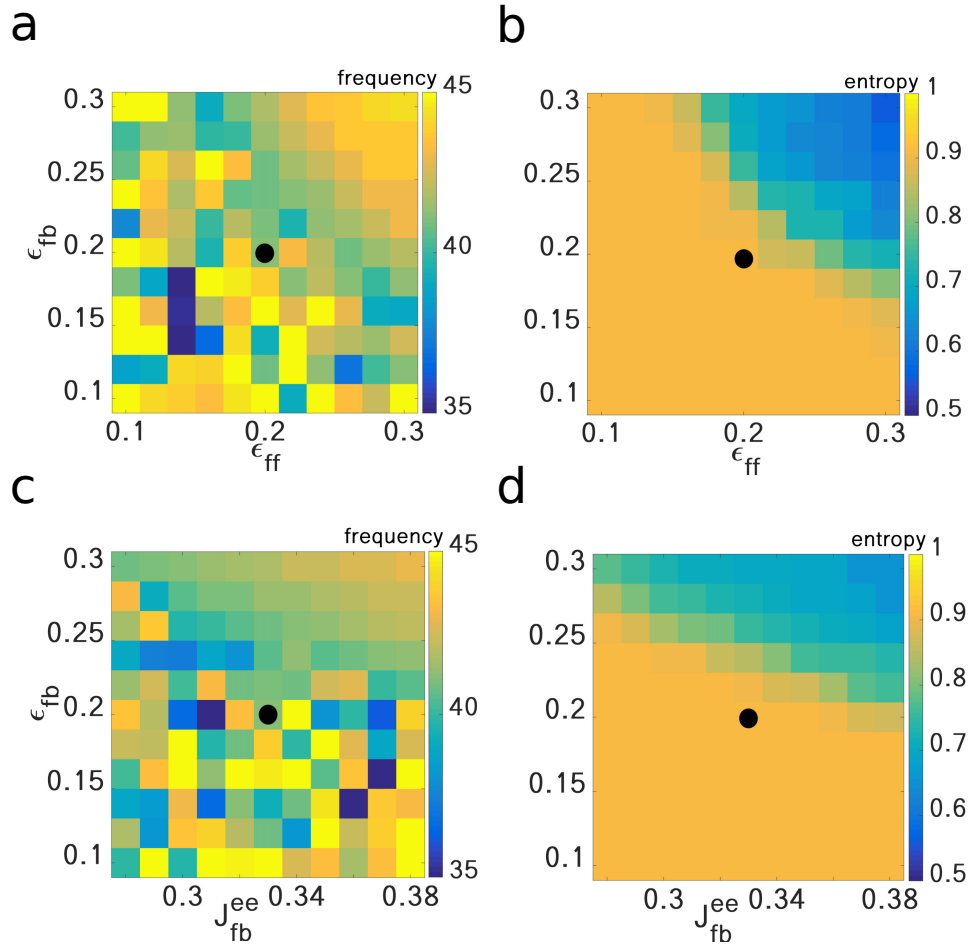


Fig 8. Conditions for resonance in a bidirectionally connected two-layer network. Network resonance frequency and spectral entropy were calculated as a function of the feedback and feedforward connection probability (a, b), and as a function of the feedback connection probability and strength (c, d). Both an increase in the feedback connection probability and strength increased the propensity of the network to exhibit resonance. However, when the feedback connections were too numerous or too strong, the network exhibited sustained oscillations as the network dynamics bifurcated to the synchronous irregular state. This state, represented by lower values of spectral entropy in (b) and (d), started with a population oscillation frequency of around 40 Hz, which gradually increased to 43 Hz (a, c). Note that at higher values of spectral entropy, the frequency of the oscillations was not well-defined and did not have a consistent value. Black circles in all four panels indicate the parameter set used in **Figures 2, 3** and **6** for investigating the pulse packet propagation in the absence of sustained oscillations.

Discussion

374

Neuronal networks in the brain show a modular structure at multiple spatial scales. Computation in the nervous system is carried by the flow of signals through a hierarchy of such modules via convergent-divergent feedforward projections. Such connectivity provides the network with a rich computational repertoire and forms the basis of models of sensory processing systems [36–38] and deep neural network models [39].

375
376
377
378
379

But brain networks are not purely feedforward structures. Neurons within the modules are interconnected by recurrent connections and there is also an abundance of feedback projections between the various modules (e.g. [25, 29]). Each module in the neocortex consists of a complex network of excitatory and inhibitory neurons, giving rise to rich internal network dynamics which may affect the transmission of signals between the modules. Depending on a variety of internal and external parameters [33, 34], *EI*-networks may show oscillatory collective dynamics, either spontaneously or in response to external transient stimuli. Such oscillatory network dynamics modulate the excitability of the module over time, thereby providing windows of high excitability during which incoming signals have a higher chance of eliciting a spiking response in the target module and, hence, to be transmitted along the modular hierarchy [8, 10, 15].

380
381
382
383
384
385
386
387
388
389
390

Feedback projections are quite ubiquitous in the central nervous system [28], and their role in regulating neuronal network activity [40, 41], brain activity oscillations [42–44], and high level brain functions such as working memory [45], vision [46, 47], attention [48, 49], and consciousness [50–52] is widely studied. Here, we studied how feedback connections can help improve the propagation of synchronous spiking activity in feedforward neuronal networks. We showed that including a pair of bidirectionally connected modules into an otherwise feedforward network promotes the propagation of synchronous spike volleys in the network. In our layered network model, each module was a recurrent network of excitatory and inhibitory neurons, tuned to operate in an asynchronous-irregular state [33, 34]. Such *EI*-networks in the *AI* state have been earlier shown to exhibit a damped oscillatory population activity in response to external transient stimulation [15, 53–55]. This property was exploited to support the propagation of synchronous spiking activity in an FFN consisting of modular *EI*-networks by a mechanism called *communication through resonance (CTR)* [15]. In this mechanism, a periodic train of pulse packets, the intervals of which matched the period of the damped resonance oscillation of the module networks, could propagate along the feedforward network, whereas a single pulse packet could not.

391
392
393
394
395
396
397
398
399
400
401
402
403
404
405
406
407

Here, we showed that single pulse packets can propagate in the network by adding feedback projections between the first two layers of the feedforward network.

408
409

Reverberation of the transient stimulus between the first two layers of the network, the resonance pair, fed the downstream remainder of the network with a temporally coordinated and strong train of pulse packets, with inter-packet intervals determined by the sum of the forward and backward transmission delays of the resonance pair. Hence, matching the two internal time scales of the system, the resonance period of the module networks and the loop transmission delay of the resonance pair, sufficed to help a single pulse packet propagate reliably across the entire network through the built-in CTR mechanism. Indeed, in a series of simulation experiments we could demonstrate that in our network model, the consistency of the two time scales, determined by the lateral (recurrent), feedforward and feedback connections, facilitates the transmission of transient synchronous spiking signals.

410
411
412
413
414
415
416
417
418
419
420

The possible role of feedback connections in the propagation of synchronous pulse packets through modular networks has been studied before [56]. There, it was shown that feedback connections increased the number of spikes in the synchronous spike volley and, thereby, helped the pulse packet propagate in the feedforward network [56]. That mechanism, however, operates on a much shorter time scale than the one we

421
422
423
424
425

propose here. In their model [56], propagation was facilitated by feedback delays within the temporal spread of the injected pulse packet, i.e., up to only few milliseconds. The mechanism we propose here is both qualitatively and quantitatively different and is based on the resonance property of the *EI*-networks involved in the feedforward network. Here, the impact of a pulse packet on the target *EI*-network provides, thanks to the damped resonance oscillation it evokes, a short range of specific time windows with enhanced excitability and, hence, larger response to the next incoming pulse packet. As a result, the reverberation of the pulse packet between the bidirectionally connected layer networks in the resonance pair builds up even stronger pulse packets for the downstream, feedforward layers of the network. We found that a prerequisite for successful propagation of such synchronous spiking activity was that the loop transmission delay in the resonance pair (forward plus feedback delay) matched the resonance period of the individual layer *EI*-networks.

It has been shown before that spike signals can be transmitted along networks in the brain in the form of spike rate [57] or spike synchrony [58–61]. Computational studies have shown that spike rate transmission requires sparse and strong synaptic connections, whereas spike synchrony transmission favors weak and dense synaptic connections [7]. Both these conditions are unlikely to be fulfilled in biological cortical networks, in which connections are typically weak and sparse [62]. The results of our study show that the presence of only a moderate degree of feedback projections between two cortical areas considerably weakens the conditions for propagating synchronous spiking activity through a much longer sequence of cortical areas. Since the necessary condition for long-range transmission of synchronous spiking signals is the presence of feedback connections only between the first two networks involved, the proposed mechanism needs only low wiring cost [63] and is an economically favorable way for efficiently organizing the communication between neuronal networks in the brain. The ubiquity of feedback connections between cortical areas (e.g. [25–30]) provides a further strong argument in favor of such scheme. In view of this ubiquity, we hypothesize that bidirectionally connected cortical areas may provide good broadcasters of information in the brain at intermediate and larger spatial scales.

Recent studies have suggested different functional roles of high and low frequency oscillations in bottom-up and top-down signaling in cortical networks [9,64]. It has been shown that the transmission of information along the feedforward pathway from peripheral sensory areas to higher areas in the cortical hierarchy is mainly carried by gamma range oscillations, whereas feedback signals are mostly conveyed by alpha and/or beta oscillations [9,65–67]. These results gained support from experimental observation of strongest synchronization in the gamma band in superficial cortical layers, whereas synchronization in the alpha-beta band was found to be strongest in infragranular layers [68]. In our network model, the baseline activity of the layer networks lacked spontaneous oscillations, but they exhibited a resonance property in the low-gamma range. The presence of a single feedback loop with matching loop delay resulted in short-lived gamma oscillations upon transient stimulation of the first layer network, resulting in reliable signal propagation throughout the entire feedforward pathway, consistent with the above-mentioned experimental observations. Incorporating further feedback loops between more downstream layer networks can provide a more complete model for explaining forward and backward signaling in cortical networks of networks.

Acknowledgments

Partial funding of this work by the German Federal Ministry of Education and Research (BMBF) grant 01GQ0830 to the Bernstein Focus Neurotechnology (BFNT) Freiburg/Tuebingen, the Carl Zeiss Foundation, the MSRT (Ministry of Science,

Research, and Technology) of Iran, and the Iran Saramadan Elmi Federation (ISEF) is gratefully acknowledged. The authors acknowledge support by the State of Baden-Württemberg through bwHPCand the German Research Foundation (DFG) through grant no INST 39/963-1 FUGG (bwForCluster NEMO), and especially to Uwe Grauer and Bernd Wiebelt for helping making these HPC-facilities available to us.

476
477
478
479
480

References

1. Modha DS, Singh R. Network architecture of the long-distance pathways in the macaque brain. *Proc Nat Acad Sci.* 2010;107:13485–13490.
2. Binzegger T, Douglas RJ, Martin KA. A quantitative map of the circuit of cat primary visual cortex. *J Neurosci.* 2004;24(39):8441–8453.
3. Xu X, Olivas ND, Ikrar T, Peng T, Holmes TC, Nie Q, et al. Primary visual cortex shows laminar-specific and balanced circuit organization of excitatory and inhibitory synaptic connectivity. *The J of Physiology.* 2016;594(7):1891–1910.
4. Boucsein C, Nawrot M, Schnepel P, Aertsen A. Beyond the cortical column: abundance and physiology of horizontal connections imply a strong role for inputs from the surround. *Frontiers in neuroscience.* 2011;5:32.
5. Schnepel P, Kumar A, Zohar M, Aertsen A, Boucsein C. Physiology and impact of horizontal connections in rat neocortex. *Cerebral Cortex.* 2014;25:3818–3835.
6. Meunier D, Lambiotte R, Bullmore ET. Modular and hierarchically modular organization of brain networks. *Front Neurosci.* 2010;4(200).
7. Kumar A, Rotter S, Aertsen A. Spiking activity propagation in neuronal networks: reconciling different perspectives on neural coding. *Nat Rev Neurosci.* 2010;11:615–627.
8. Hahn G, Ponce-Alvarez A, Deco G, Aertsen A, Kumar A. Portraits of communication in neuronal networks. *Nature Rev Neurosci.* 2018;20:117–127.
9. Engel AK, Fries P, Singer W. Dynamic predictions: oscillations and synchrony in top-down processing. *Nature Rev Neurosci.* 2001;2:704–716.
10. P F. A mechanism for cognitive dynamics: neuronal communication through neuronal coherence. *Trends Cogn Sci.* 2005;9:474–480.
11. Vogels TP, Abbott LF. Gating multiple signals through detailed balance of excitation and inhibition in spiking networks. *Nature Neurosci.* 2008;12(4):483–491.
12. P F. Neuronal gamma-band synchronization as a fundamental process in cortical computation. *Annu Rev Neurosci.* 2009;32:209–224.
13. Kremkow J, Perrinet LU, Masson GS, Aertsen A. Functional consequences of correlated excitatory and inhibitory conductances in cortical networks. *J Comput Neurosci.* 2010;28:579–594.
14. Kremkow J, Aertsen A, Kumar A. Gating of signal propagation in spiking neuronal networks by balanced and correlated excitation and inhibition. *J Neurosci.* 2010;30(47):15760–15768.

15. Hahn G, Bujan AF, Fregnac Y, Aertsen A, Kumar A. Communication through resonance in spiking neuronal networks. *PLOS Comput Biol.* 2014;10(8).
16. Pariz A, Esfahani ZG, Parsi SS, Valizadeh A, Canals S, Mirasso CR. High frequency neurons determine effective connectivity in neuronal networks. *NeuroImage.* 2018;166:349–359.
17. Abeles M. Role of cortical neuron: integrator or coincidence detector? *Isr J Med Sci.* 1982;18:83–92.
18. Diesmann M, Gewaltig M, Aertsen A. Stable propagation of synchronous spiking in cortical neural networks. *Nature.* 1999;402:529–533.
19. Gewaltig M, Diesmann M, Aertsen A. Propagation of cortical synfire activity: survival probability in single trials and stability in the mean. *Neural Netw.* 2001;14:657–673.
20. Aertsen A, Diesmann M, Gewaltig M. Propagation of synchronous spiking activity in feedforward neural networks. *J Physiol.* 1996;90:243–247.
21. Abeles M. Neural Circuits of the Cerebral Cortex. *Corticonics.* 1991;.
22. Burns SP, Xing D, Shapley RM. Is gamma-band activity in the local field potential of v1 cortex a ‘clock’ or filtered noise? *J Neurosci.* 2011;31:9658–9664.
23. Palmigiano A, Geisel T, Wolf F, Battaglia D. Flexible information routing by transient synchrony. *Nature Neurosci.* 2017;20(7):1014.
24. Sanristobal B, Vicente R, Garcia-Ojalvo J. Role of frequency mismatch in neuronal communication through coherence. *J Comp Neurosci.* 2014;37(2):193–208.
25. Felleman SJ, Essen DC. Distributed hierarchical processing in the primate cerebral cortex. *Cereb Cortex.* 1991;1:1–46.
26. Stephan KE, Kamper L, Bozkurt A, Burns GA, Young MP, Kotter R. Advanced database methodology for the Collation of Connectivity data on the Macaque brain(CoCoMac). *Philos Trans R Soc Lond B Biol Sci.* 2001;356:1159–1186.
27. Bakker R, Thomas W, Diesmann M. CoCoMac 2.0 and the future of tract-tracing databases. *Front Neuroinformatics.* 2012;6(30).
28. Markov NT, Ercsey-Ravasz MMea. A weighted and directed interareal connectivity matrix for macaque cerebral cortex. *Cerebral Cortex.* 2014;24(1):17–36.
29. Mejias JF, Murray JD, Kennedy H, Wang XJ. Feedforward and feedback frequency-dependent interactions in a large-scale laminar network of the primate cortex. *Science Advances.* 2016;2(11):e1601335.
30. Schmidt M, Bakker R, Hilgetag CC, Diesmann M, van Albeda SJ. Multi-scale account of the network structure of macaque visual cortex. *Brain Struct Funct.* 2018;223:1409–1435.
31. Gewaltig MO, Diesmann M. NEST (NEural Simulation Tool). *Scholarpedia.* 2007;2(4):1430.

32. Morrison A, Straube S, Plesser HE, Diesmann M. Exact subthreshold integration with continuous spike times in discrete-time neural network simulations. *Neural Comput.* 2007;19:47–79.
33. Brunel N. Dynamics of sparsely connected networks of excitatory and inhibitory spiking neurons. *J Comput Neurosci.* 2000;8(3):183–208.
34. Kumar A, Schrader S, Aertsen A, Rotter S. The high-conductance state of cortical networks. *Neural Computation.* 2008;20:1–43.
35. Kumar A, Rotter S, Aertsen A. Conditions for propagating synchronous spiking and asynchronous firing rates in a cortical network model. *J Neurosci.* 2008;28:5268–5280.
36. Riesenhuber M, Poggio T. Hierarchical models of object recognition in cortex. *Nat Neurosci.* 1999;2:1019–1025.
37. Serre T, Oliva A, Poggio T. A feedforward architecture accounts for rapid categorization. *Proc Natl Acad Sci.* 2007;104(15):6424–6429.
38. Dicarlo JJ, Zoccolan D, Rust NC. How does the brain solve visual object recognition? *Neuron.* 2012;73(3):415–434.
39. LeCun Y, Bengio Y, Hinton G. Deep learning. *nature.* 2015;521(7553):436.
40. Hauptmann C, Popovych O, Tass PA. Delayed feedback control of synchronization in locally coupled neuronal networks. *Neurocomputing.* 2005;65:759–767.
41. Hashemi M, Valizadeh A, Azizi Y. Effect of duration of synaptic activity on spike rate of a Hodgkin-Huxley neuron with delayed feedback. *Physical Review E.* 2012;85(2):021917.
42. Contreras D, Destexhe A, Sejnowski TJ, Steriade M. Control of spatiotemporal coherence of a thalamic oscillation by corticothalamic feedback. *Science.* 1996;274(5288):771–774.
43. Bazhenov M, Timofeev I, Steriade M, Sejnowski TJ. Model of thalamocortical slow-wave sleep oscillations and transitions to activated states. *J Neurosci.* 2008;22(19):8691–8704.
44. Rosenblum M, Pikovsky A. Delayed feedback control of collective synchrony: an approach to suppression of pathological brain rhythms. *Physical review E.* 2004;70(4):041904.
45. Tanaka S. A prefronto-parietal network model with feedforward and feedback connections. *Neurocomputing.* 2002; p. 943–948.
46. Shou TD. The functional roles of feedback projections in the visual system. *Neurosci Bull.* 2010;26:401–410.
47. Kafaligonul H, Breitmeyer BG, Ogmen H. Feedforward and feedback processes in vision. *Frontiers in Psychology.* 2015;6.
48. Miconi T, VanRullen R. A feedback model of attention explains the diverse effects of attention on neural firing rates and receptive field structure. *PLOS Comp Biol.* 2016;12(2: e1004770).

49. Macknik SL, Martinez-Conde S. Role of feedback in visual attention and awareness. *Consciousness*. 2009; p. 1165–1179.
50. Lamme VAF. Blindsight: the role of feedforward and feedback corticocortical connections. *Acta Psychologica*. 2001;107(1):209–228.
51. Bullier J. Feedback connections and conscious vision. *Trends in Cognitive Sciences*. 2001;5:369–405.
52. Clavagnier S, Falchier A, Kennedy H. Long-distance feedback projections to area V1: Implications for multisensory integration, spatial awareness, and visual consciousness. *Cognitive Affective and Behavioral Neuroscience*. 2004;4:117–126.
53. Mehring C, Hehl U, Kubo M, Diesmann M, Aertsen A. Activity dynamics and propagation of synchronous spiking in locally connected random networks. *Biol Cybern*. 2003;88:395–408.
54. Ledoux E, Brunel N. Dynamics of networks of excitatory and inhibitory neurons in response to time-dependent inputs. *Front Comput Neurosci*. 2011;5(25).
55. Shin D, Cho KH. Recurrent connections form a phase-locking neuronal tuner for frequency-dependent selective communication. *Scientific Reports*. 2013;3(2519).
56. Moldakarimov S, Bazhenov M, Sejnowski TJ. Feedback stabilizes propagation of synchronous spiking in cortical neural networks. *Proc Natl Acad Sci*. 2015;112(8):2545–2550.
57. Vogel A, Ronacher B. Neural correlations increase between consecutive processing levels in the auditory system of locusts. *J Neurophysiol*. 2007;97:3376–3385.
58. Doupe AJ. Cellular, circuit, and synaptic mechanisms in song learning. *Ann NY Acad Sci*. 2004;1016:495–523.
59. Kao MH, Wright BD, Doupe AJ. Neurons in a forebrain nucleus required for vocal plasticity rapidly switch between precise firing and variable bursting depending on social context. *J Neurosci*. 2008;28:13232–13247.
60. Kimpo RR, Theunissen FE, Doupe AJ. Propagation of correlated activity through multiple stages of a neural circuit. *J Neurosci*. 2003;23:5750–5761.
61. Kojima S, Doupe AJ. Activity propagation in an avian basal ganglia-thalamocortical circuit essential for vocal learning. *J Neurosci*. 2009;29:4782–4793.
62. Seeman SC, Campagnola L, Davoudian PA, Hoggarth A, Hage TA, Bosma-Moody A, et al. Sparse recurrent excitatory connectivity in the microcircuit of the adult mouse and human cortex. *Elife*. 2018;7:e37349.
63. Sporns O, Tononi G, Kotter R. The human connectome: A structural description of the human brain. *PLoS Comput Biol*. 2005;1:245–251.
64. Bonnefond M, Kastner S, Jensen O. Communication between Brain Areas Based on Nested Oscillations. *eNeuro*. 2017;4(2):e0153–16.
65. Chalk Mea. Attention reduces stimulus-driven gamma frequency oscillations and spike field coherence in V1. *Neuron*. 2010;66:114–125.

66. Sarter M, Hasselmo ME, Bruno JP, Givens B. Unraveling the attentional functions of cortical cholinergic inputs: Interactions between signal-driven and cognitive modulation of signal detection. *Brain Res Rev.* 2005;48:98–111.
67. Yu AJ, Dayan P. Uncertainty, neuromodulation, and attention. *Neuron.* 2005;46:681–692.
68. Buffalo EA, Fries P, Landman R, Buschman TJ, Desimone R. Laminar differences in gamma and alpha coherence in the ventral stream. *Proc Nat Acad Sci.* 2011;108:11262–11267.

Table 1. Neuron parameters

Name	Value	Description
C_m	250 pF	Membrane capacitance
G_{leak}	16.67 nS	Membrane leak conductance
Θ	-54 mV	Spiking threshold
V_{reset}	-70 mV	Reset potential
τ_{ref}	2 ms	Refractory time period

Table 2. Synapse parameters

Name	Value	Description
τ_{exc}	1 ms	Rise time of excitatory synaptic conductance
τ_{inh}	1 ms	Rise time of inhibitory synaptic conductance
E_{syn}^{exc}	0 mV	Reversal potential of excitatory synapses
E_{syn}^{inh}	-80 mV	Reversal potential of inhibitory synapses
J_{ee}	0.33 mV	Exc. to exc. synaptic strength measured at -70 mV
J_{ei}	1.5 mV	Exc. to inh. synaptic strength measured at -70 mV
J_{ie}	-6.2 mV	Inh. to exc. synaptic strength measured at -54 mV
J_{ii}	-12.0 mV	Inh. to inh. synaptic strength measured at -54 mV
J_{pe}	0.25 mV	Synaptic weight. Input Poisson spike train to exc. population
J_{pi}	0.4 mV	Synaptic weight. Input Poisson spike train to inh. population
J_{pp}	0.33 mV	Synaptic strength from pulse packet to P neurons in layer I
$d_{within-layer}$	1.5 ms	Transmission delay within layer
$d_{inter-layer}$	25 - 28 ms	Range of total resonance delay between layers

Table 3. Network parameters

Name	Value	Description
N_{exc}	200	Size of excitatory population per layer network
N_{inh}	50	Size of inhibitory population per layer network
N_{proj}	70	Number of projecting neurons per layer network
$\epsilon_{within-layer}$	0.2	Connection probability within-layer network
$\epsilon_{inter-layer}$	0.2	Connection probability between layer networks

Supporting information

Statistical analysis of three different background activity regimes in Figure 7.

Distributions of CV_{ISI} , correlation coefficients, and firing rates for three background activity regimes of the two network structures FFN and RPN are shown in **Supplementary Figure S1**. Consistent with previous Figures, red traces represent the RPN network structure, blue traces the FFN. Increasing Poisson input rate and inter-layer connection strengths from top to bottom resulted in lower mean values of the CV_{ISI} distributions (left column), indicating more regular spike timing. Moreover, the CV_{ISI} distributions became distinctly narrower, indicating more homogeneity among the neurons' background spiking irregularities in both network types. Neurons also showed higher correlation coefficients as the Poisson input rate and inter-layer connection strengths increased (middle column), indicating increasing synchrony among the excitatory neurons in each network type. Moreover, in the top two panels the correlation coefficient distributions of the two network types more or less overlapped, but in the bottom panel they became clearly distinct, with considerably higher background activity correlations in the RPN than in the FFN. Finally, neurons tended to fire at higher rates when exposed to higher input rates and stronger inter-layer connections, resulting in an unbalanced state (right column). Also here, the firing rate distributions of the two network types more or less overlapped in the top two panels, but in the bottom panel they became clearly distinct, with considerably higher firing rates in the RPN than in the FFN. Thus, from a spike statistics point of view, the differences between the background activities of the FFN and RPN became most obvious in the high-rate spiking regime (bottom row, marked with a square).

Raster plots for the three regimes of background network activity in both network types are also shown in **Supplementary Figure S2**, in the same color code (blue for FFN, red for RPN). As is clearly visible, increasing external Poisson input rate and inter-layer connection strengths gradually shifted the background network activity from an asynchronous irregular activity state toward synchronous oscillations.

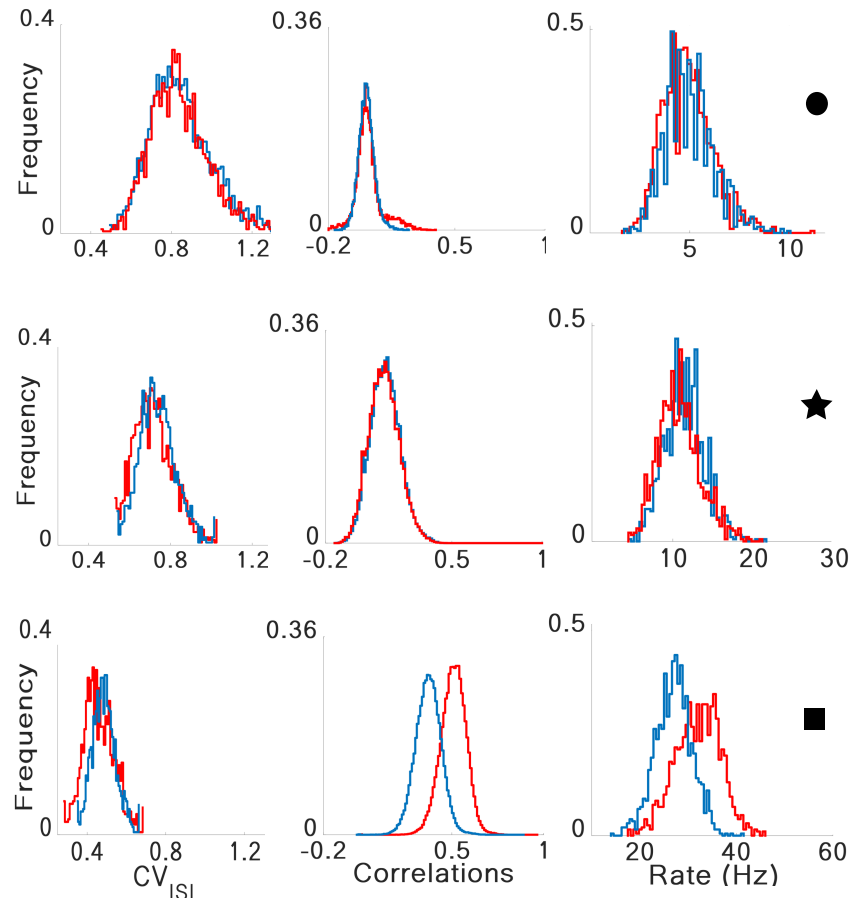


Fig S1. Distributions of CV_{ISI} , pair-wise correlations, and firing rates of excitatory neurons in three different background firing regimes of the RPN and FFN. Distributions of CV of inter-spike intervals (left), pairwise correlations (middle), and firing rates (right) for three different sets of external input and inter-layer connection strengths. Red and blue traces denote RPN and FFN network structures, respectively. Three states are introduced in **Figure 7** with corresponding markers. For weak external inputs and inter-layer connection strengths, the network in both structures exhibited asynchronous irregular activity. In this state, adding excitatory feedback connections did not affect the network activity states. However, when the network was operating in a synchronous irregular activity state (corresponding to the higher external excitatory input and stronger inter-layer synapses, bottom row, indicated with a black square) adding feedback connections resulted in increased firing rates and synchrony indices, even more so in the RPN than in the FFN (compare red and blue traces in the two right-most panels in the bottom row), while spiking became distinctly more regular in both network types (left panel).

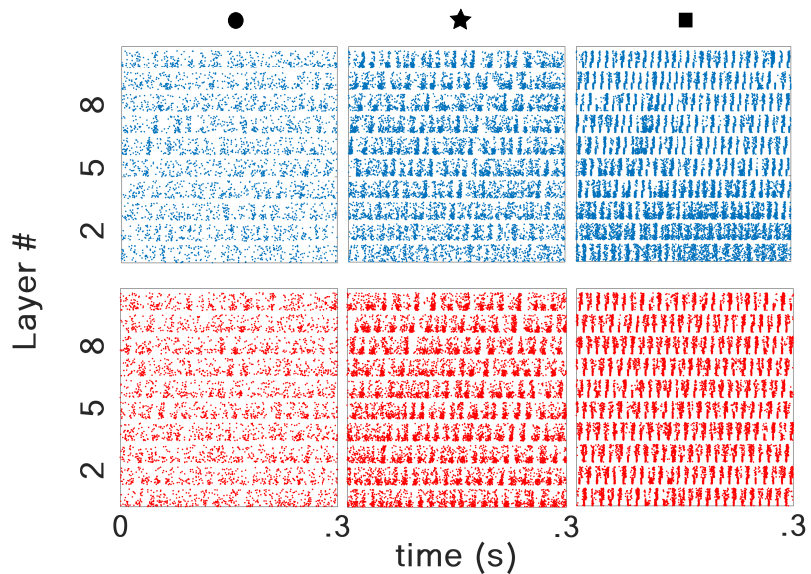


Fig S2. Raster plots for three different background firing regimes of the **RPN** and **FFN**. Increasing input rate and inter-layer connection strength both increased the propensity of the RPN and the FFN to synchronize their background activities. For the regime marked with the black square (rightmost column), both networks showed network activity oscillations.